High-quality vascular modeling and modification with implicit extrusion surfaces for blood flow computations

Qingqi Hong[a], Qingde Li[b], Beizhan Wang[a], Jie Tian[c], Fei Xu[a], Kunhong Liu[a,*], Xuan Cheng[a,*]

[a]*School of Informatics, Xiamen University, Xiamen, China*
[b]*School of Engineering and Computer Science, University of Hull, UK*
[c]*Institute of Automation, CAS, Beijing, 100190, China*

Abstract

Background and Objective: High-quality vascular modeling is crucial for blood flow simulations, i.e., computational fluid dynamics (CFD). As without an accurate geometric representation of the smooth vascular surface, it is impossible to make meaningful blood flow simulations. The purpose of this work is to develop high-quality vascular modeling and modification method for blood flow computations. **Methods:** We develop a new technique for the accurate geometric modeling and modification of vasculatures using implicit extrusion surfaces (IES). In the proposed method, the skeleton of the vascular structure is subdivided into short curve segments, each of which is then represented implicitly locally as the intersection of two mutually orthogonal implicit surfaces defined by distance functions. A set of contour points is extracted and fitted with an implicit curve for accurately specifying the vessel cross-section profile, which is then extruded locally along the skeleton to fill the gaps between two vascular tube cross sections. We also present a new implicit geometric editing technique to modify the constructed vascular model with pathology for virtual stenting. **Results:** Experimental results and validations show that accurate vascular models with highly smooth surfaces can be generated by the proposed method. In addition, we conduct some blood flow simulations to indicate the effectiveness of proposed method for hemodynamic simulations. **Conclusions:** The proposed technique can achieve precise geometric models of vasculatures with any required degree of smoothness for reliable blood flow simulations.

Keywords: Geometric Modeling, Vascular Visualization, Implicit Functions, Blood Flow Simulation, Extrusion Surfaces

1. Introduction

As reported by World Health Organization (WHO) in 2017, there were almost 17,900,000 people suffered from vascular diseases during 2016, taking up 31% of the global deaths [43]. These vascular system malfunctions generally occur from arteriosclerosis and have a high possibility of developing vascular stenosis or occlusion, which has a significant threat to human health. Particularly, internal carotid artery (ICA) stenosis leads to insufficient intracranial perfusion, which is considered as the leading cause of stroke [42].

With the development of computer graphics and medical imaging technology, 3D models of vasculatures can be reconstructed from scanned medical images, which is of great help in many clinical applications for the treatment of vascular diseases, such as diagnosis of vascular stenosis, vascular surgery planning, simulations of interventional procedures, blood flow computations, and so on. Firstly, by reconstructing the vascular geometric model, the location of the lesion can be located more preciously, and more importantly, various quantitative analysis can be performed, which is difficult or even impossible to carry out based on the initial discrete data points. Secondly, an accurate, smooth and realistic vessel model is essential for

*Corresponding Author: Kunhong Liu, Xuan Cheng.
E-mail address: hongqq@gmail.com (Q.Hong), lkhqz@xmu.edu.cn (K.Liu), 21408732@qq.com (X.Cheng).

the simulation of insertion and navigation in interventional procedures. In addition, the highly smooth and accurate reconstruction for vessel geometries is a crucial step for the simulation of patient-specific blood flows, to maintain numerical computational stabilities and guarantee correct simulation results [38]. Simulations of blood flows based on patient-specific geometries enable us to perform research on hemodynamic characteristics associated with specific patients [30, 21, 20, 9, 34], which can help doctors in choosing optimal treatment therapies.

Generally, automatic vessel segmentation is a traditional way to acquire vascular geometry from medical images, and various techniques have been developed in the past few decades. However, the initial segmented data is generally expressed as discrete polygonal meshes, which is not suitable for many clinical applications of vascular surgery [22]. The reconstructed vessel surface is expected to be highly smooth and can be expressed in an analytical form, which is very useful during the vascular analysis phase. Specifically, accurate vascular models with sufficient degree of smoothness are crucial for performing trusty blood flow simulations, which could be quite difficult to be achieved based on segmentation results. Hence, the focuses of this paper are on reconstructing faithful and smooth vascular models from the segmented point sets, as well as developing an implicit geometry editing technique for easy adjustments of the reconstructed models to simulate stenting treatment option.

In this paper, a new tubular shape modeling technique is proposed for the accurate geometry reconstruction of vasculatures based on implicit extrusion surfaces (IES). Firstly, each cross-section profile is specified using 2D implicit splines in the form of weighed sum of locally constructed implicit geometric primitives. Then each implicitly represented 2D cross-section profile is then extruded into 3D implicit surfaces along an implicit extrusion path. In the following, by employing the 1D partial shape-preserving spline (PSPS) functions, all the implicit extrusion surfaces are weighted and summed up together to construct a long implicit extrusion surface. Our method is applied to real vascular images, and is able to construct a smooth, C^{m-1} $(m \geq 2)$ continuous vascular shape expressed mathematically in analytic form. We also present a new implicit geometric editing technique to modify the constructed vascular model with pathology for virtual stenting, which is a common intervention method for treating artery stenosis. Experimental results indicate the generated vessel models are of high quality and accuracy. Furthermore, quantitative analysis has been carried out to validate the accuracy and smoothness of the constructed vessel models. We also conduct some blood flow simulations based on the constructed and reshaped vascular models with pathology to evaluate our proposed method's effectiveness.

2. Related work

2.1. Geometric Modeling of Vascular Structures

In recent years, many researchers have carried out numerous studies on the patient-specific geometric modeling of vasculatures [41, 35], and developed some relevant modeling toolkits [18]. Generally, current geometric modeling techniques for vasculatures can be categorized to be *explicit modeling-based methods* and *implicit modeling-based methods*.

Explicit methods represent vascular models by using explicit polygonal meshes or parametric functions, which are relatively mature and efficient for rendering. Polygonal mesh is one of the most popular geometry presentations for modeling vascular structures, such as cylinders [31], truncated cones [11], subdivision mesh [10, 46], simplex meshes [6], curvature-dependent surface [44], and so on. However, the generated surface of vasculatures is very complicated so that the higher accuracy means the more tiny meshes, more computing time, and more consumed memory. Besides, the meshing method has a poor performance at handling branching structure modeling [4]. In the other type of explicit modeling method, vascular surface is represented by parametric functions, i.e., B-spline or NURBS (Non-Uniform Rational B-Splines). For instance, Höhne et al. [13] proposed an explicit modeling method to build small vessel structures as well as tiny nerves by B-spline functions. However, because the vascular structure is particularly complicated, the vasculature may be represented by a large number of curves. Therefore, repairing geometric and topological errors has also become an important task in this field, aiming at achieving local connections, global topologies and geometries [2]. An improved approach based on ball B-Spline curves is presented in Wang et al.'s work

[42] for the repairing of cerebral vascular structures from MRA data. Zhang et al. [48] presented an modeling method based on hexahedral solid NURBS surface to generate geometric models of vasculatures for computing blood flows. A NURBS curve blending technique was presented by Liu et al. [28] to achieve G^2 continuity without changing the original shape of the curves. Generally, it is a challenging task for explicit methods to deal with shape blending and branching [4]. A more accurate and case-specific connection of sets of polygons or parametric patches is required for smooth transitions at branching, such as the semi-tubular sweeping method to construct bifurcation junctions [12].

Implicit modeling methods, in contrast, represent the geometric model of vasculatures as implicit functions. The geometric shape defined by an implicit function could be considered an isovalue representing the density of interest, which is inherently easy to combine in various ways. Because of this, implicit modeling owns an inherent composition mechanism to implement ramification in a simple way. In particular, unlike combining two mesh-represented geometric objects, implicitly defined geometric shapes, when blended together, are free of unwanted inner parts, which is crucial for conducting reliable blood flow simulations [22].

Various implicit modeling techniques have been presented for the geometric modeling of vasculatures, which is able to implement smooth transitions at the branch point. Oeltze and Preim [32] proposed a famous approach for visualizing vascular structure based on convolution surfaces (CS) [5]. Although the CS-based method can achieve excellent visualization results of vessel structures, it is not suitable to model vascular structures with pathology, due to its oversimplified assumption that all cross sections are circular. Schumann et al. [39, 38] proposed a model-free method for visualizing vasculatures based on multi-level partition of unity implicits (MPUI) [33]. Although the MPUI-based method is able to generate accurate implicit vascular surfaces, the generated surface's quality is not as good as that based on CS method, which needs an additional remeshing step for improvement [38]. In order to reach good balance between fitting accuracy and the smoothness of the fitted surface, Wu et al. [45] developed a scale-adaptive surface modeling method for the effective geometric modeling of vascular structures, which is based on a 3D implicit indicator function computed from the segmented 3D point cloud by solving a Poisson equation. A local implicit modeling technique was proposed by Kerrien et al. [19] to construct vascular models, which improved Bittar et al. and Tsingos et al.'s work [3, 40] by expressing the fitting problem as an energy minimization approach to avoid unwanted blending and gain smoothness as well as versatility.

Another popular way of implicit modeling method for constructing vascular structures is based on sweep surfaces, which represents the vessel cross-section as a 2D spline curve while using the generalized cylinder paradigm to sweep surfaces [15]. Hong et al. [15] developed an implicit technique for reconstructing the geometry of vasculatures, which combined a sweep step of bivariate piecewise algebraic splines (PAS) [25] and polynomial blending at ramifications, and performed the whole vessel tree with a global blending function. Although the PAS-based method can model vessel tree with high smoothness properties, the modeling accuracy might be affected when the vascular skeleton has a high curvature. A method for modeling vasculatures using sweep surfaces was proposed by Kretschmer et al.[22], to generate high-quality vascular models and modify the incorrect vessel segmentations at interactive frame rates. However, the vascular models generated by this method have only C^1 continuity. Recently, Hong et al. [16, 17] utilized the fitting approach with radial basis functions [27] to construct accurate vascular models with high smoothness. However, the vascular models generated by radial basis fitting technique cannot be directly expressed in an analytical form.

2.2. Geometric modification of vessel models

In comparison with the geometric modeling of vasculatures, there are only several researches that are devoted to the modification of individualized vessel models, aiming at estimating and evaluating the surgical outcomes [47]. Saalfeld et al. [37] developed an user interface based on sketch, which allowed physician to simulate different treatment methods for various vascular diseases. However, this work represents the vessels and blood flow in 2D, which is sufficient only for the purpose of education. Ding [7] developed a cardiovascular surgery virtual modeling tool, to simulate the operations of bypass and patch, and tried to optimize the geometry of the bypass graft through hemodynamic optimization. Appanaboyina et al. [1] proposed a hybrid meshing method to map different stenting designs to a given vascular model, for the

purposes of evaluating the outcomes of endovascular treatment for cerebral aneurysms. Xiong et al. [47] developed triangle-based geometric methods for virtually deploying stent grafts to individualized vascular models, which allowed the user to interactively reshape the preoperative models to access the geometric effects of different interventions.

However, all the above mentioned techniques for the geometric modification of vascular structures are based on explicitly represented geometries. The underlying geometric model of vasculatures and stents are expressed either as a triangular surface or as NURBS functions, and it is a difficult task to perform geometric editing (e.g. surface blending) and optimizing operations [29].

3. Material and methods

3.1. Tubular shape modeling using implicit extrusion surfaces

In this subsection, we develop a tubular shape modeling method based on implicit extrusion surfaces, which can be directly applied to reconstruct from a volumetric medical image the geometry of tubular structures of certain human organs, such as blood vessels, ureters, lung tracheas, depending on the type of medical image is used. To build the entire tubular surface geometry, we first analytically represent each 2D cross-section dataset as piecewise bivariate algebraic spline $B^{(m)}_{\triangle,\delta}(x,y)$ [25], which is able to construct a continuous curve with explicit mathematical analytic expression to accurately approximate the irregular cross-section profile captured by each cross-section dataset. Each of these 2D implicit curves is then extruded locally along an extrusion path. The extrusion is done implicitly by representing a skeleton segment around each cross-section locally as two implicit surfaces perpendicular to each other. Finally, we employ the 1D partial shape-preserving spline (PSPS) functions [26] to construct a tubular shape model along a given centreline as the weighted sum of all locally extruded implicit surfaces, which has varying cross-sectional profiles and explicit mathematical expression.

3.1.1. Implicit extrusion

An implicit surface can be generated by implicit extrusion, of which the basic idea is to represent the curve along which a 2D implicit curve is extruded as the intersection of two implicit surfaces. More specifically, let the implicit curve be represented implicitly by $X(x,y,z)=0$ and $Y(x,y,z)=0$, and let $f(x,y)=0$ be a 2D implicit function representing the cross-section profile of an implicit shape. Then the implicitly extruded geometric shape is expressed as $f(X(x,y,z),Y(x,y,z))=0$. A rich set of implicit surface can be defined in this way. However, when the two implicit surfaces used for specifying the extrusion path are not defined as distance functions or not mutually orthogonal, the profile defined by $f(x,y)=0$ will be deformed when it is extruded along the intersection curve of the two surfaces as shown in Figure 1. The shape in (a) is generated by extruding the circle $f(x,y)=x^2+y^2=0$ along the intersection line of two mutually orthogonal planes: $X(x,y,z)=-3x+y=0$ and $Y(x,y,z)=z=0$. As $-3x+y=0$ is not a distance function, the initial profile is distorted. The shape in (b) is generated by extruding the same 2D profile along the intersection of the same two planes, where the implicit function $X(x,y,z)=-3x+y=0$ representing the first plane is replaced with a distance function $X1(x,y,z)=(-3x+y)/sqrt(10)=0$.

It is also easy to see that even though the two implicit functions used for specifying the extrusion path are both distance functions, if they are not orthogonal, that is, their normal vector fields are not perpendicular to each other, the profile will also be deformed during the extrusion process. Thus, to maintain the 2D cross-section profile unchanged during the process of extrusion, the two implicit surfaces used for specifying the extrusion path must be orthogonal and must be represented in distance functions.

However, it is a practically challenging task to specify the extrusion path as the orthogonal intersection of two implicit surfaces defined by distance functions [24]. In general, apart from a few simple geometric primitive curves, it is difficult to express a given space curve as the intersection of two mutually orthogonal implicit surfaces represented in distance functions. Our solution to the problem is to adaptively subdivide a given curve into short curve segments, such that each of which can be well approximated as quadratic algebraic or piecewise quadratic algebraic curves. There are two reasons why quadratic curves are chosen to solve the problem in our method. First, all quadratic curves are planar as they can be interpreted as the

(a) (b)

Figure 1: Extrusion of an implicitly defined 2D circle along an implicit curve defined by two planes: $X(x,y,z) = -3x + y = 0$ and $Y(x,y,z) = z = 0$. (a) Extrusion path defined by $X(x,y,z)$ and $Y(x,y,z)$, (b) Extrusion path defined by $X1(x,y,z)$ and $Y(x,y,z)$, where $X1 = (-3x + y)/sqrt(10) = 0$ is a distance function corresponding to the plane represented by $X(x,y,z)$

.

intersection of a plane with a cone. Thus, we can always turn the problem of finding orthogonal surfaces in 3D as a 2D problem by transforming each 3D quadratic curve to a 2D coordinate plane. As a 2D implicit curve can always be viewed as the intersection of 3D cylindrical surface with a coordinate plane, the task of computing two distance function-represented orthogonal implicit surfaces virtually becomes a task of finding the distance function of a 2D curve. The second reason behind our choice is directly related to the task of representing a curve in 2D as a distance function. Compared with other 2D curves, representing a 2D quadratic curve as a distance function is much simpler, in some cases, even closed-form solution is available. Thus, the use of quadratic curve segments to approximate the initial skeleton curve makes it easy to solve this tough problem locally.

Here are the main steps of the proposed method:

1. Adaptively subdivide the skeleton of a tubular shape (represented by a parametric curve $\mathbf{S}(s)$) into a set of segments corresponding to $s = s_0, s_1, \cdots, s_{N-1}$, such that the accumulated torsion and curvature of each skeleton segment corresponding to parametric interval $[s_i, s_{i+1}]$ is less than a given value $\epsilon > 0$, which is calculated numerically based on the formula shown below:

$$\int_{s_i}^{s_{i+1}} \sqrt{\kappa^2 + \tau^2} ds < \epsilon \tag{1}$$

where κ is the curvature and τ is the torsion of the skeleton (please refer to [36] for the detail definition of κ and τ). In addition, it is assumed that the length of each skeleton segment is not larger than a predefine threshold L, which is indicated by the number of the interpolated-spline points of the parametric skeleton $\mathbf{S}(s)$. That is, controlled by ϵ and L, each skeleton segment will be neither too curved nor too long. Generally, the values of ϵ and L parameters can be set to [8, 60] and [80, 600] respectively in our experiments. It should be noted that, when the ϵ is set large enough, the length of each skeleton segment will be only determined by L, which can be considered as the uniform skeleton subdivision approach. Figure 2 presents an example of subdividing a skeleton using our adaptive method, which produces skeleton segments with varying lengths.

2. Suppose $\mathbf{S}(s_i)(x,y,z)$ is the centre point of a skeleton segment in $\boldsymbol{R}^3$ space, then each point on this segment can be projected on the normal plane of the Frenet frame defined at $\mathbf{S}(s_i)$. In other words, the skeleton segment is projected on the **TB**-plane of the local coordinate system defined by $\mathbf{T}$, $\mathbf{B}$, $\mathbf{N}$ at $\mathbf{S}(s_i)$ (Figure 3). Suppose $\mathbf{S}(s_j)(x,y,z)(j = 1,2,3,...,N)$ are skeletal points in $\boldsymbol{R}^3$ space and $\mathbf{S}^*(s_j)(x_{tbn}, y_{tbn}, z_{tbn})$ are skeletal points projected on the TB-plane in the local coordinate system **TBN** space, and the projected expressions are as follows:

$$\begin{cases} x_{tbn} = (\mathbf{S}(s_j) - \mathbf{S}(s_i)) \bullet \mathbf{T}(s_i) \\ y_{tbn} = (\mathbf{S}(s_j) - \mathbf{S}(s_i)) \bullet \mathbf{B}(s_i) \\ z_{tbn} = 0 \end{cases} \tag{2}$$

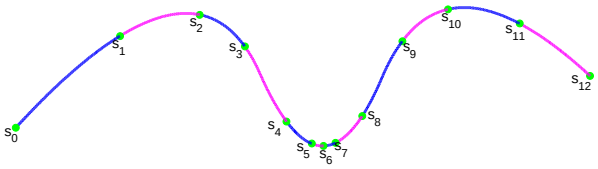

Figure 2: An example of adaptive subdivision of a skeleton, where the skeleton segments produced from our adaptive skeleton subdivision scheme are marked by a set of green points on the given skeleton curve.

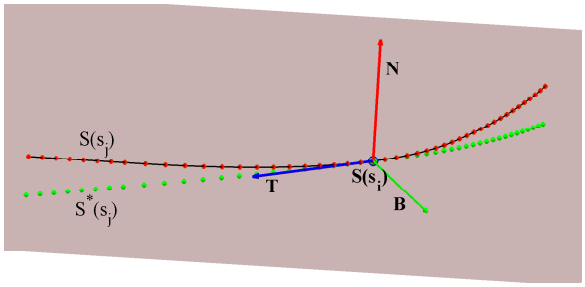

Figure 3: A skeleton segment is projected on the **TB**-plane of the local coordinate system defined by **T**, **B**, **N** at the centre point of the segment.

3. A polynomial curve $f_c(x_{tbn}, y_{tbn}) = y_{tbn} - \rho(x_{tbn}) = 0$ is fitted to the projected points $\mathbf{S}^*(s_j)(j = 1, 2, 3, ..., N)$ on the **TB**-plane in the local coordinate system **TBN**. Generally, $\rho(x)$ is a quadratic polynomial fitted by least squares. In the space defined by the local coordinate system $\mathbf{TBN}(x_{tbn}, y_{tbn}, z_{tbn})$, the extrusion path can be implicitly represented as the intersection of the two implicit surfaces: $f_c(x_{tbn}, y_{tbn}) = y_{tbn} - \rho(x_{tbn}) = 0$ and the normal plane $z_{tbn} = 0$, where $f_c(x, y)$ is a 2D quadratic curve (Figure 4) .

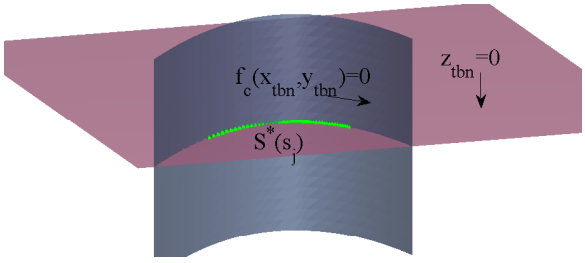

Figure 4: The extrusion path implicitly represented as the intersection of two implicit surfaces $f_c(x_{tbn}, y_{tbn}) = 0$ and $z_{tbn} = 0$.

4. Suppose in the Frenet-frame space $\mathbf{BNT}(x_{bnt}, y_{bnt}, z_{bnt})$, the cross-section profile is defined as an implicit spline function $C_i(x_{bnt}, y_{bnt})$=$B^{(m)}_{\triangle,\delta}(x_{bnt}, y_{bnt})$-h=0, and $f_x(x_{bnt}, y_{bnt}, z_{bnt}) = f_c(x_{tbn}, y_{tbn}) = 0$, $f_y(x_{bnt}, y_{bnt}, z_{bnt}) = z_{tbn} = 0$, then the extruded implicit surface along the extrusion path (Figure 5) can be directly given by:

$$\begin{aligned} f_i(x_{bnt}, y_{bnt}, z_{bnt}) &= C_i(x_{bnt}, y_{bnt}) = C_i(f_c(x_{tbn}, y_{tbn}), z_{tbn}) \\ &= C_i(f_x(x_{bnt}, y_{bnt}, z_{bnt}), f_y(x_{bnt}, y_{bnt}, z_{bnt})) \\ &= 0 \end{aligned} \tag{3}$$

where $i = 1, 2, 3, ..., N$.

5. The implicit extrusion surface represented in the Frenet-frame space $\mathbf{BNT}(x_{bnt}, y_{bnt}, z_{bnt})$ can be transformed to $\boldsymbol{R}^3$ space by performing a distance mapping, of which expression is denoted as the following

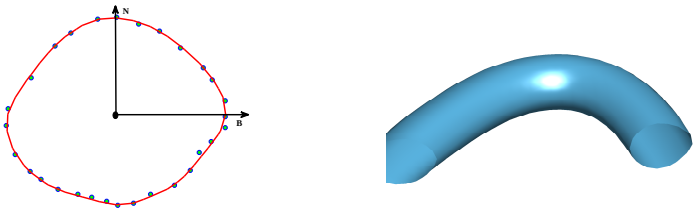

(a) (b)

Figure 5: An implicit extrusion surface is constructed by extruding a cross-section profile along the implicit extrusion path defined in Figure 4. (a) The cross-section profile, (b) The implicit extrusion surface.

equation:

$$\begin{cases} x_{bnt} = X(x, y, z) \\ y_{bnt} = Y(x, y, z) \\ z_{bnt} = Z(x, y, z) \end{cases} \tag{4}$$

Please refer to the Appendix for details about the distance mapping.

3.1.2. Constructing the tubular shape model with varying cross-section profiles using 1D PSPS functions

All the implicit extrusion surfaces (IES) generated by extruding a specified cross-section profile are weighted and summed up together along a given centreline to construct a long implicit extruded surface (Figure 6). To preserve locally extruded implicit shapes, the 1D PSPS functions $B_i(z)$ [26] is used to perform weighted superposition along a given centreline to construct a complete tubular model with varying cross sections $C_i(x, y)$. The expression of the entire model is as follows:

$$\begin{aligned} f(x_{bnt}, y_{bnt}, z_{bnt}) &= \sum_{i=1}^{L} C_i(f_x(x_{bnt}, y_{bnt}, z_{bnt}), f_y(x_{bnt}, y_{bnt}, z_{bnt}))B_i(z_{bnt}) \\ &= 0 \end{aligned} \tag{5}$$

From Equation 4, it can be seen that $(x_{bnt}, y_{bnt}, z_{bnt})$ are all function of (x, y, z). That is, the constructed tubular model in $\boldsymbol{R}^3$ space can be given by:

$$\begin{aligned} F(x, y, z) &= f(x_{bnt}, y_{bnt}, z_{bnt}) \\ &= f(X(x, y, z), Y(x, y, z), Z(x, y, z)) \\ &= 0 \end{aligned} \tag{6}$$

3.2. Accurate geometric modeling of vasculatures based on IES

In this subsection, we apply the proposed tubular modeling method to the geometric modeling of vasculatures. The idea behind our method involves two steps: the extraction of the vascular skeleton, and the extraction of a list of cross-section profile points from the vessel surface along the skeleton. The extraction of skeleton is based on the work [14], which moves an exploring sphere along the vessel tree to detect skeletal points step by step. The extraction of the contour points for specifying vessel cross-section profile will be presented in the following subsection.

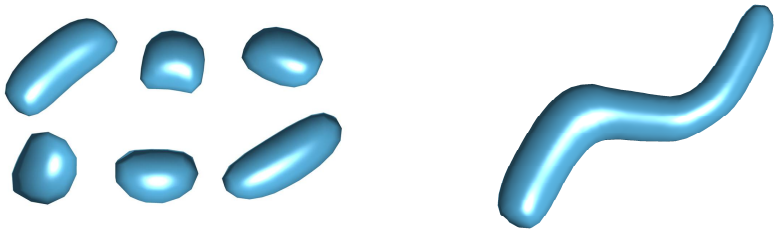

(a) (b)

Figure 6: Different implicit extrusion surfaces (IES) generated by a 2D specified cross-section profile (a) are weighted and summed up together along a given centreline to construct a long implicit extrusion surface (b).

(a) (b)

Figure 7: Move a defined rectangle (a) to the centre point of a skeleton segment and intersect with the vascular surface (b).

3.2.1. Control point extraction for specifying vascular cross-section profile

Suppose $\mathbf{S}(s_i)$ is the centre point of a skeleton segment, and $\mathbf{T}(s_i)$, $\mathbf{B}(s_i)$, and $\mathbf{N}(s_i)$ are the Tangent unit vector, Binormal unit vector, and Normal unit vector on the Frenet frame at $\mathbf{S}(s_i)$ respectively, then the main steps of extracting the control points that depict the cross-section profile based on $\mathbf{S}(s_i)$ are as follows:

1. Move a defined rectangle to the centre point of a skeleton segment to intersect perpendicular to the vascular surface (Figure 7). The translation steps include:

(a) Rotate the local z-axis on the defined rectangle (Figure 7 (a)) and make it parallel to the Normal unit vector $\mathbf{N}(s_i)$;

(b) Rotate the local x-axis and y-axis around the local z-axis on the defined rectangle (Figure 7 (a)) and make them parallel to the Tangent unit vector $\mathbf{T}(s_i)$ and Binormal unit vector $\mathbf{B}(s_i)$ respectively;

(c) Translate the centre point of the rectangle to the position of $\mathbf{S}(s_i)$.

2. Map the intensity value of the vascular segmentation data into the defined rectangle, and extract the contour points that have zero intensity value for specifying the vascular cross-section profile. The hybrid level-set segmentation method [49] is used to identify the vessel regions from raw medical images. After segmentation, the intensity values of bright pixels are greater than zero, which indicates the inside area of vascular structures. On the other hand, the intensity values of black pixels are smaller than zero, which indicates the outside area of vascular structures. Sometimes, we cannot find the pixel with zero value in the boundary of the vessel. In this case, we use the linearly interpolated points along grid point edges as the contour points. The extracted contour points are marked in red colour. (Please see Figure 8 (a))

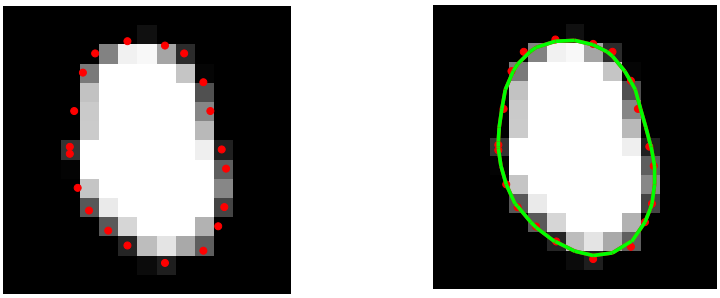

(a) (b)

Figure 8: (a) The intensity value of the vascular segmentation data is mapped into the defined rectangle, then the contour points that have zero intensity value are extracted as the control points; (b) 2D implicit spline function is employed for faithfully representing the cross-section profile based on the extracted contour points.

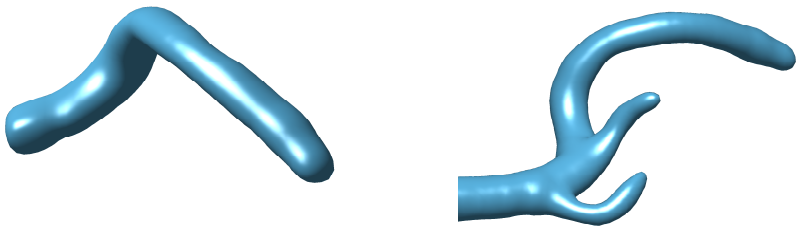

(a) (b)

Figure 9: (a) A vascular branch model is constructed with our IES-based method; (b) Three different vascular branching models are combined with the smooth shape-preserving maximum function.

3.2.2. Main steps of vascular modeling based on IES

Once the vessel tree's skeleton has been extracted, we can reconstruct the geometric model of vascular structures by using the proposed IES-based tubular shape modeling method. The specific process is as follows:

1. For a given branch of vessel tree, we subdivide its skeleton $S_j(s)$ into several short segments based on the method described in step (1) of subsection 3.1.1. The segment length is implied by the interpolated-spline point number of the parametric skeleton $S_j(s)$.

2. For each skeleton segment, we construct the local **BNT** coordinate system based on its centre point $S_j(s_i)$, and draw out the control points for the specification of the cross-section profile at $S_j(s_i)$ (please refer to subsection 3.2.1). Then, 2D implicit spline function is employed for faithfully representing the cross-section profile based on the extracted control points (Figure 8 (b)).

3. Using the method presented in subsection 3.1.1, the 2D implicit curves representing cross-section profiles are extruded into 3D implicit surfaces. Then, by adopting the 1D PSPS function, all the IES are weighted and summed up together along the skeleton to construct the complete vascular branch model (Figure 9 (a)).

4. Finally, in order to achieve bulge-free blending of bifurcation, we employ the smooth shape-preserving

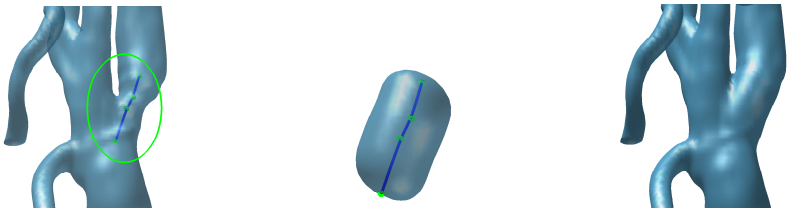

(a) (b) (c)

Figure 10: Virtual stenting based on implicit modeling method: (a) the identified diseased portion and its skeleton , (b) the constructed cylindrical shape F_S representing the stented model based on the skeleton and radius R , (c) the modified vascular model of post-operative with stenting.

maximum function $max_{n,\delta}(x, y)$ [23] to combine different vascular branching models implicitly constructed from different central lines $\mathbf{S}_j(s)(j = 1, 2, 3, ..., N)$ together to build the whole vessel tree. Suppose F_1 and F_2 are two implicitly-defined vessel models, smooth blending of these two implicitly expressed shapes can be implemented by the following expression:

$$F_{blend} = max_{n,\delta}(F_1, F_2) = \frac{1}{2}(F_1 + F_2 + |F_1 - F_2|_{n,\delta}) \tag{7}$$

in which $|.|_{n,\delta}$ is the smooth absolute function with degree of smoothness n and blending range-control parameter δ defined in [23]. As shown in Figure 9 (b), three different vascular branching models are combined with the smooth shape-preserving maximum function to achieve bulge-free blending of bifurcation.

As can be seen from the above steps, in the proposed IES-based vascular modeling method, the representation of vascular cross-sectional profile, the locally extruded implicit surfaces, the generated tubular model, and the different branching models produced by the shape-preserving blending operation, are all expressed mathematically in an analytical form. Thus, the generated patient-specific vascular models based on IES method have an analytical mathematical expression, which is able to guarantee C^{m-1} $(m \geq 2)$ continuity for the generated vascular surfaces and facilitates subsequent operations such as vessel shape analysis, hemodynamic simulations, surgery planning and simulations of vasculatures.

3.3. Geometric modification for pathological vasculatures

Artery stenosis is one of the most common vascular diseases, and the commonly used treatment is stent implantation, in which a stent is set up into a section of the artery to expand the stenosis. In surgery planning, we can implement virtual stenting by editing the geometry of the reconstructed vascular model, and carry out hemodynamic simulations based on the reshaped models to illustrate the effectiveness of the treatment planning for diseased vasculatures. Unlike explicitly modeling technique, implicit modeling technique provides an inherent way to represent solid objects, which is much easier to perform geometric editing operations based on implicitly represented geometric models. The virtual stenting to treat artery stenosis can be easily implemented based on the proposed implicit modeling technique. The main steps are as follows:

1. Input a reconstructed vascular model and recognize the pathological portion to be reshaped by virtual stenting;

2. Choose two endpoints by the user to identify the skeleton segment of the diseased portion (see Figure 10 (a));

3. Calculate the radius R of the cylindrical shape representing the stented model by taking the average of two radii of the contours corresponding to the two endpoints of the skeleton segment;

4. Specify a 3D implicit cylindrical shape F_S by using the proposed IES-based method, which extrudes an implicit circle with radius R along the skeleton segment to construct the required stented model (see Figure 10 (b));

5. Blend the constructed stented model F_S with the original vascular model F_O to construct the virtual stented vascular model (see Figure 10 (c)) with the shape-preserving maximum function:

$$\max_{n,\delta}(F_O, F_S) = \frac{1}{2}(F_O + F_S + |F_O - F_S|_{n,\delta}) \tag{8}$$

Generally, the radius of the vessel stenosis part is smaller than that of the cylindrical stent, and the shape of the stent model will not be affected when blending with the vessel of smaller radius based on the shape-preserving maximum function $\max_{n,\delta}(x, y)$. In addition, $\max_{n,\delta}(x, y)$ is a piecewise polynomial with the smoothness degree n and blending range-control parameter δ, which allows flexible blending range specification [23]. Thus, the proposed geometric modification method is able to yield a simulation result as realistic as possible. It should be noted that, in clinical applications, we need to further communicate with the doctor to accurately determine the radius, length, placement position and other parameters of the stent.

4. Results and Discussion

4.1. Modeling results based on our proposed method

We have adopted a variety of medical datasets to test our proposed method on its effectiveness as well as robustness. This subsection will present some typical reconstruction results of vasculatures, including carotid arteries with stenosis (CarArt), cerebral vasculatures (CerVas), coronary arteries (CorArt), liver portal vein (LPVein), and popliteal arteries with aneurysm (PopArt), which represent the characteristic vascular structures of human vasculature system. The information concerning the presented datasets is summarized in Table 1.

Table 1: Summary of the information concerning the presented datasets. Voxel sizes are given in millimeters

Datasets	Resolution	Voxel size
CarArt	$512 \times 512 \times 149$	$0.52 \times 0.52 \times 0.63$
CerVas	$352 \times 442 \times 114$	$0.49 \times 0.49 \times 0.80$
CorArt	$512 \times 512 \times 295$	$0.40 \times 0.40 \times 0.45$
LPVein	$512 \times 512 \times 310$	$0.70 \times 0.70 \times 0.63$
PopArt	$123 \times 118 \times 400$	$0.83 \times 0.83 \times 1.00$

As presented in Figure 11, subfigure (a) is the direct visualization of segmentation result of carotid arteries, and subfigure (b) is the modeling result based on the proposed method. A visual comparison between the segmentation result and our modeling result gives us the first evidence that our proposed method can correctly represent the topology and morphology of vascular structures. Besides, extremely thin branches and complicated vascular structures (Figure 12) can be rebuilt faithfully using our technique. In addition, Figure 13 presents a detailed look at the modeling results f pathological vasculatures. As can be seen from the ellipse areas, pathological vasculatures with aneurysm or stenosis can be faithfully modelled by the proposed method.

4.2. Comparison with PAS-based approach

PAS-based approach is a skeleton based implicit modeling technique, which is able to achieve excellent model quality of reconstructed vasculartures. Both the PAS-based technique and the proposed technique are developed based on a series of points sampled along the vascular skeleton. The two methods differ mainly in the way the locally fitted cross-section profiles are extended to 3D and combined together. With PAS-based method, the local Frenet frame for the skeleton at each sampled point is used to build an orthonormal basis,

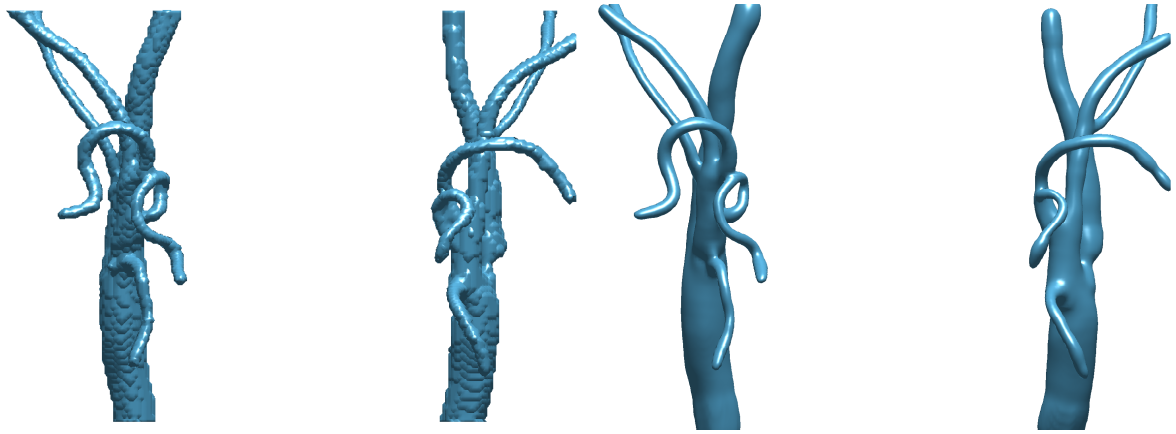

(a) (b)

Figure 11: The modeling result of CT carotid arteries. (a) The direct visualization of segmentation result, (b) The modeling result based on the proposed method.

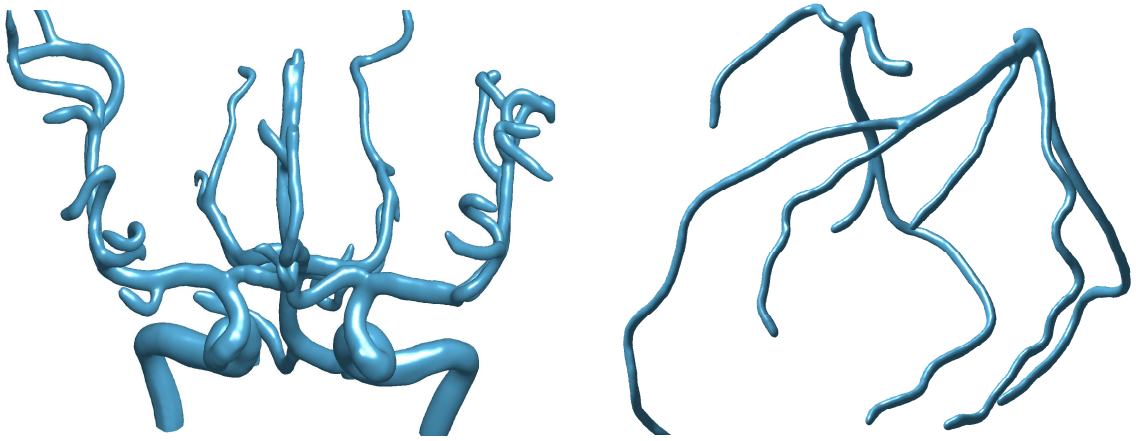

(a) (b)

Figure 12: Some of the modeling results using our method. (a) MRA cerebral vasculatures, (b) CT coronary arteries.

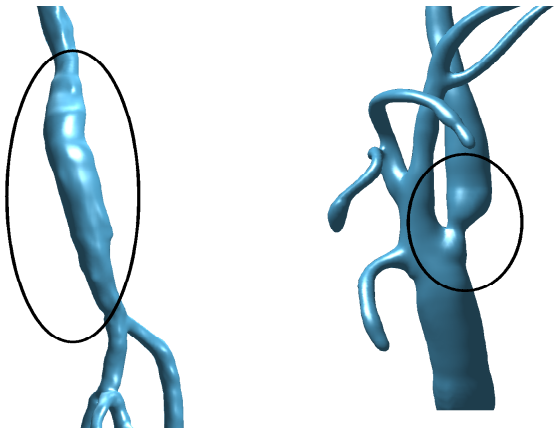

(a) (b)

Figure 13: A detailed look at the modeling results of pathological vasculatures. (a) Popliteal arteries with aneurysm, (b) Carotid arteries with stenosis.

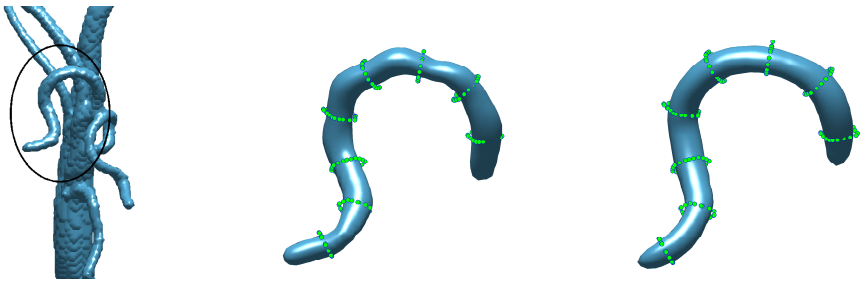

(a) (b) (c)

Figure 14: The comparison between the proposed technique and PAS-based technique for modeling a vessel branch with high curvature. (a) The segmented vascular tree that contains a branch with high curvature (indicated by the ellipse), (b) The generated model of the curved branch using PAS-based technique, (c) The generated model of the curved branch using our technique.

and the locally fitted 2D cross-section profile is extended to 3D through distance mapping by transforming the relative points into the local Frenet frame space. A curved skeleton was considered as consisting of several straight-line segments and a 2D specified cross-section profile is swept along a straight-line segment to generate a sweep surface, all of which are blended together to build a curved tubular model.

This method works very well at the place where the local skeleton curve is relatively flat. However, when the skeleton of a vessel branch is very curved, the accuracy of the reconstructed model is often greatly affected (Figure 14 (b)). Thus, the distance between two skeletal points for defining Frenet frame should be set quite small to guarantee the smooth blending of different cross-section profiles. However, when the distance between two cross-section profiles is set very small, it often leads to the problem of cross-section self intersections.

On the other hand, our proposed method has a good solution to solve the problem caused by the much curved skeleton line. In our method, a 2D specified cross-section profile is extruded into 3D implicit surface along an extrusion path, which can be implicitly represented as the intersection of two distance function-defined surfaces. For any given curved centreline, our method is able to construct appropriate extrusion paths for generating the smooth implicit extrusion surfaces. Figure 14 illustrates the comparison between the proposed technique and PAS-based technique for modeling a vascular branch with high curvature. The implicit extruded surface achieved by our method is of great smoothness, while that generated by PAS-based method undergoes severe unsmoothness and disjointedness.

4.3. Quantitative validation

To verify the validity of the proposed modeling method, some quantitative analysis and investigation have been conducted.

The Euclidean distances between the modelled vascular surface and the segmentation result are used to evaluate the accuracy, which are measured in the following way: firstly, both the surface points of the segmentation result and our modelled vascular surface are extracted as two point sets; then the distances between the closest points from each point set are calculated. Generally, the modeling accuracy of the proposed method could be affected by the subdivided skeleton segment length L. In order to investigate the modeling effect concerning different skeleton segment configurations, we present the median of the distances (Med) based on the modeling results with different L.

Figure 15 reports the detail Med values measured on the modeling results generated by both PAS-based method and our IES-based method with different lengths of skeleton segments (indicated by horizontal coordinate) for each experimental dataset. As can be seen from the figure, the Med values of both methods are generally the same when L is small. As L becomes larger, the Med deviations of PAS-based method grow much faster than that of IES-based method. In other words, the model accuracy of the IES-based method is much less affected by the segment length than the PAS-based method.

In addition, other statistical measures, such as the mean of the distance (Mean), the root mean square distance (Rms) and the maximum distance (Max), are also calculated for the comprehensive evaluation of accuracy; while the averaged unsigned mean curvatures (AUMC) [8] of the reconstructed surface is considered as the criterion of surface smoothness.

We conduct a direct quantitative comparison between the proposed IES-based technique and PAS-based technique, 2D RBF-based technique [16], and MPUI-based technique [38] for vessel modeling of different datasets. Table 2 records the averaged statistical measures for each dataset, among which the distance values are in millimetres when considering the accuracy. Generally, IES-based method has the smallest measured values (Mean and Med) for each experimental datasets, which means that the proposed technique is able to generate more accurate vascular models than the other techniques do. As far as smoothness is concerned, it can be measured by the AUMC value: the smaller AUMC value demonstrates that an approach has the ability of reconstructing much smoother surface. Among these four methods, the AUMC values based on the IES method are the smallest, which is below 0.24 for each dataset. In a word, as presented in the table, the IES-based technique has a better performance than the other compared implicit modeling techniques, which is able to achieve accurate vascular models with excellent smoothness property.

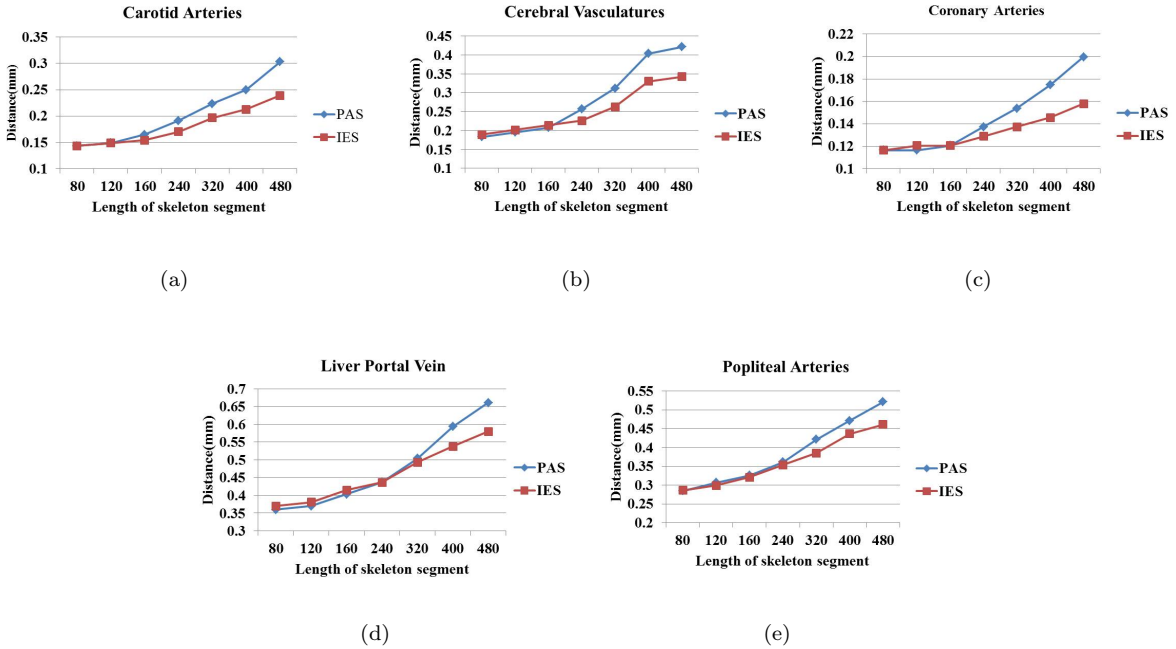

Figure 15: The detail Med values measured on the modeling results generated by both PAS-based method and our IES-based method with different lengths of skeleton segments (indicated by horizontal coordinate) for different datasets: (a) carotid arteries; (b) cerebral vasculatures; (c) coronary arteries; (d) liver portal vein; (e) popliteal arteries.

4.4. Time complexity

Generally, the efficiency of the proposed modeling approach could be affected by the resolution of input dataset and the complexness of the vascular structures, as well as the skeleton segment length L. Generally, the complexness of the vascular structure can be reflected by the number of triangular faces generated from the implicitly represented models for visualization. Table 3 summarizes information concerning the geometric complexity of the resulting models and the performance of our method when L is set as 240. Currently, the modeling process is totally based on CPU computation, of which the computational cost is relatively high. However, as implicit modeling is a parallel computing friendly geometric reconstruction technique, the computational performance of the proposed method could be greatly improved by taking advantage of parallel architecture of modern programmable GPUs.

4.5. Blood flow simulation for pathological vasculatures

In this subsection, an example of blood flow simulation based on the constructed and modified vascular models from a patient dataset with vessel disease is presented to demonstrate the impact of blood flow dynamics on the diseased vascular wall. We apply the proposed implicit modeling method to the geometric reconstruction of carotid artery with stenosis for the 3D CTA images. As stated in [38], a smooth geometric representation is crucial for blood flow computation to avoid numerical instabilities and guarantee correct simulation results. Thus, a post-processing step is designed to enhance the triangle quality of the vessel surfaces genetrated by MPUI-based method [38]. On the other hand, our method can faithfully represent the stenosis of internal carotid artery (ICA) branch and achieve highly smooth surfaces (Figure 16 (a)), without any additional remeshing step. In addition, the implicitly represented vascular model can be easily modified using our implicit editing technique, to implement the virtual stenting for treating the stenosis of carotid artery (Figure 16 (b)).

The geometric model defined by an implicit function can be considered an isosurface representing the density of interest. When the function value equals to a certain threshold, it corresponds to the model

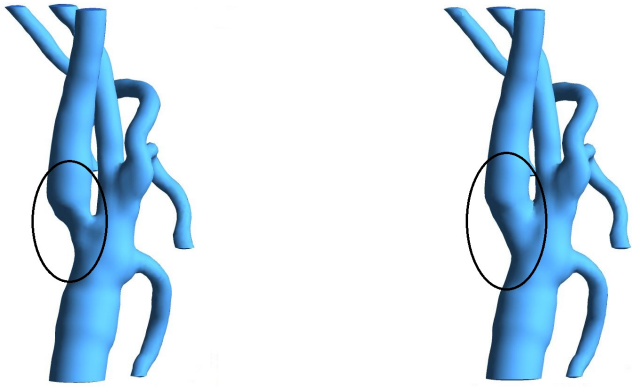

(a) (b)

Figure 16: The geometric modeling and modification of carotid artery with stenosis. (a) The original reconstructed model with a significant stenosis at the beginning of ICA branch , (b) The modified models with stenting. The diseased portion is identified with black ellipse.

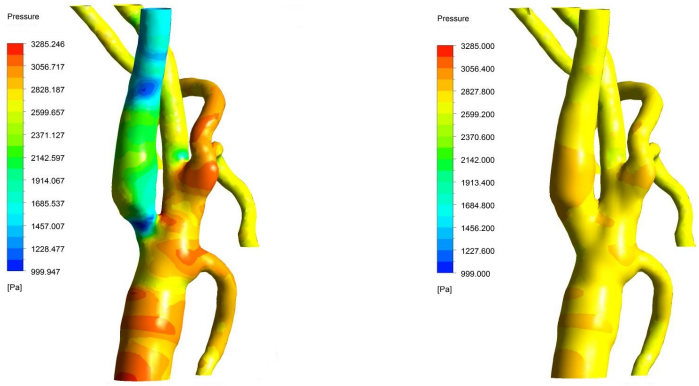

(a) (b)

Figure 17: The wall pressure of the original reconstructed model (a), and the modified models with stenting (b).

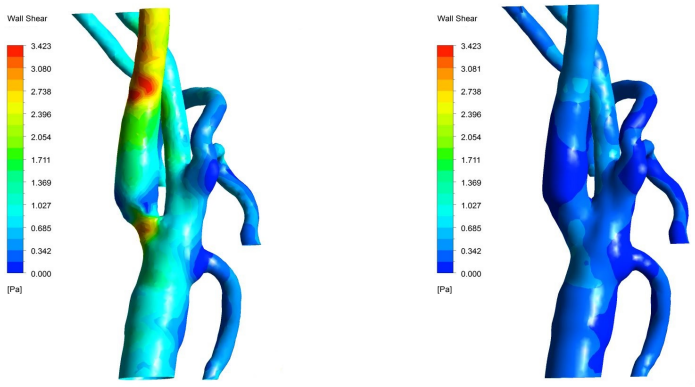

(a) (b)

Figure 18: The mean wall shear stress of the original reconstructed model (a), and the modified models with stenting (b).

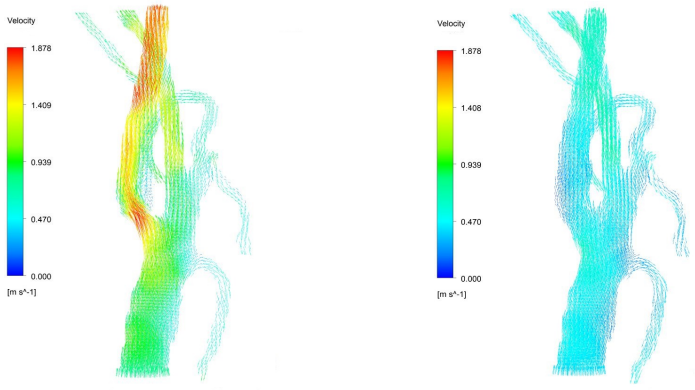

(a) (b)

Figure 19: The simulated blood velocity of the original reconstructed model (a), and the modified models with stenting (b).

Table 2: Quantitative comparison between the proposed IES-based technique and other techniques for the geometric modeling of vasculatures for different datasets. The accuracy is measured by calculating the Euclidean distances between modelled vascular surface and the segmented data, and the smoothness is estimated by measuring the AUMC of the modelled surface. Distance values are in millimetres.

Data sets	Methods	Mean	Med	Rms	Max	AUMC
CarArt	IES-based technique	0.23	0.18	0.30	1.86	0.20
	PAS-based technique	0.25	0.20	0.31	1.63	0.22
	2D RBF-based technique	0.25	0.20	0.34	2.22	0.23
	MPUI-based technique	0.26	0.26	0.27	1.28	0.28
CerVas	IES-based technique	0.33	0.25	0.45	3.09	0.21
	PAS-based technique	0.37	0.28	0.50	2.80	0.21
	2D RBF-based technique	0.34	0.26	0.46	3.93	0.22
	MPUI-based technique	0.34	0.31	0.52	7.58	0.41
CorArt	IES-based technique	0.16	0.13	0.20	1.89	0.23
	PAS-based technique	0.17	0.15	0.21	1.58	0.24
	2D RBF-based technique	0.18	0.14	0.26	2.97	0.25
	MPUI-based technique	0.22	0.22	0.24	1.41	0.44
LPVein	IES-based technique	0.66	0.46	1.00	9.04	0.13
	PAS-based technique	0.67	0.47	1.01	9.04	0.14
	2D RBF-based technique	0.79	0.61	1.16	8.91	0.17
	MPUI-based technique	0.61	0.59	0.65	6.76	0.29
PopArt	IES-based technique	0.78	0.62	0.99	5.37	0.21
	PAS-based technique	0.80	0.66	1.00	5.46	0.26
	2D RBF-based technique	0.80	0.65	1.03	8.02	0.31
	MPUI-based technique	0.88	0.86	0.94	4.76	0.63

surface. In order to extract the mesh surface of the geometric model from its implicit representation, the implicit function is firstly sampled and evaluated on a regular grid. Based on the pre-define grid, the zero-set contours can be extracted and assembled into polygons using Marching Cubes. After setting the outlets for each branch of carotid artery, we use Marching Cube method to generate the triangle mesh models of vascular surfaces from their implicit representations. Then the generated vascular surfaces can be directly used for volume mesh generation and blood flow computation, without having to perform additional smoothing process. A key step for blood flow computation is the setting of boundary conditions. In general, the boundary condition of common carotid artery inlet is set as velocity-inlet with a normal speed value of $0.8m/s$, and the boundary condition of all carotid artery outlets are set as pressure-outlet with a static pressure value of $20mmHg$. It is assumed that the vessel walls are rigid and with zero slipping. Finally, we choose the finite volume method as the CFD calculation method for blood flow simulations.

Figure 17 shows the mean wall pressure of the original reconstructed model and the modified models with stenting, which does not generate irregular distribution, such as cross or scatter distribution. In the original reconstructed model, there is a significant stenosis at the beginning of ICA branch, which results in the wall pressure of ICA is smaller than other branches. On the other hand, in the modified model with stenting, the blood flow supply of ICA has been greatly improved. As shown in Figure 17(b), the wall pressure distribution of the whole carotid artery is much more consistent than that in the original model.

Figure 18 shows the mean wall shear stress (WSS) of the original reconstructed model and the modified models with stenting. Just as the same with that of the wall pressure, the distribution of wall shear stress is independent of the initial entry conditions, which is closely related with the structure of the whole system model. Compared with the flat areas, the distribution of high wall shear stress is more focused on the narrow areas. In the original model, the WSS of ICA branch can reach up to $3Pa$, which is significantly higher than $1Pa$ of other branches. On the other hand, in the modified model with stenting, the WSS of ICA branch has been greatly decreased, which is basically identical to that of other branches. As shown in

Table 3: Performance measurements for the geometric modeling of vascular structures using IES-based method carried out on an Intel Core i7-7700HQ @2.8GHz and 32GB RAM.

Datasets	Resolution	Number of Triangles	Time(second)
CarArt	$512 \times 512 \times 149$	61608	54.60
CerVas	$352 \times 442 \times 114$	157546	132.31
CorArt	$512 \times 512 \times 295$	98868	81.76
LPVein	$512 \times 512 \times 310$	112716	169.69
PopArt	$123 \times 118 \times 400$	60018	71.48

Figure 18 (b), the WSS distribution of the whole carotid artery is much more consistent than that in the original model, of which WSS value is generally not higher than $0.6Pa$.

Figure 19 shows the simulated blood velocity of the original reconstructed model and the modified models with stenting. In the original model, the blood velocity of ICA branch can reach up to $1.8m/s$, which is significantly higher than $1m/s$ at other areas. On the other hand, in the modified model with stenting, the blood velocity ICA branch has been greatly decreased, which is basically identical to that of other branches. As shown in Figure 19 (b), the blood velocity value of the whole carotid artery is generally not higher than $0.8m/s$.

The simulation results were evaluated by three experienced radiologists, who unanimously affirmed the effectiveness of our proposed technique for the virtual intervention of treating artery stenosis.

5. Conclusions

A new technique is proposed for the high-quality geometric modeling and editing of vasculatures based on implicit extrusion surfaces (IES). In the proposed IES-based modeling method, a 2D specified cross-section profile is extruded into 3D implicit surface along an extrusion path, which can be implicitly represented as the intersection of two distance function-defined surfaces. For any given curved skeleton, our method is able to construct appropriate extrusion paths for generating the smooth implicit extrusion surfaces, and solve the problem of cross-section self intersections, which might be found in the implicit modeling method based on sweep surfaces. In addition, the generated patient-specific vascular models based on IES method have corresponding mathematical analytical expressions, which facilitate subsequent operations, such as vessel shape analysis, hemodynamic simulations, surgery planning of vasculatures, and so on. We also develop a new implicit geometric editing technique for easy adjustments of the reconstructed models to simulate virtual stenting for the treatment of artery stenosis. Experimental results as well as qualitative and quantitative validations show that the proposed technique can achieve precise geometric models of vasculatures with highly smooth surfaces. In addition, we have also conducted one case of blood flow simulation based on the generated vessel models to demonstrate the effectiveness of proposed method in hemodynamic simulations for diseased vascular structures.

One of our future work is to apply the developed approach to the modeling and editing of vascular geometries for the other portions of the vascular system for blood flow computations, such as virtual stent grafting based on the reconstructed models of abdominal aorta for the treatment of abdominal aortic aneurysm, and virtual stenting or bypass grafting based on the reconstructed models of coronary arteries to treat coronary artery stenosis, etc. One issue of the proposed method is that the computational complexity is relatively high. Thus, another future work will focus on improving computational performance of the proposed method. Implicit modeling is a parallel computing friendly geometric reconstruction technique. One possible solution is to take advantage of massively parallel architecture of modern programmable GPUs, say, by employing the NVIDIA CUDA framework, for the parallel computation of the proposed method, which will certainly improve the performance of our method.

Acknowledgment

We would like to thank anonymous reviewers for their constructive comments on this paper. This work was partly supported by the National Natural Science Foundation of China under Grant No.61502402, 61772023 and 61802322, the Fundamental Research Funds for the Central Universities under Grant No. 20720180073 and 20720190003, and National Key RD Program of China under Grant No. 2019QY1803.

Appendix

In this appendix, we describe the main steps of performing a distance mapping to transform the implicit surface model defined in the Frenet-frame space $\mathbf{BNT}(x_{bnt}, y_{bnt}, z_{bnt})$ to $\boldsymbol{R}^3$ space. Suppose $P(x, y, z)$ is the point in $\boldsymbol{R}^3$ space, $P^{\dagger}(x_{bnt}, y_{bnt}, z_{bnt})$ is the point in the Frenet-frame space **BNT** defined at $\mathbf{S}(s_i)$, and $P^*(x_{tbn}, y_{tbn}, z_{tbn})$ is the point in the local coordinate system **TBN**, then the steps for performing the distance mapping are as follows:

1. Establish the correspondence between $P^*(x_{tbn}, y_{tbn}, z_{tbn})$ and $P(x, y, z)$:

(a) Compute the rotation matrix M_1 to rotate z-axis to make it parallel to the Normal unit vector $\mathbf{N}(s_i)$ on the Frenet frame at $\mathbf{S}(s_i)$;

(b) Compute the rotation matrix M_2 to rotate the local x-axis and y-axis to make them parallel to the Tangent unit vector $\mathbf{T}(s_i)$, Binormal unit vector $\mathbf{B}(s_i)$ on the Frenet frame at $\mathbf{S}(s_i)$ respectively;

(c) The correspondence between $P(x, y, z)$ and $P^*(x_{tbn}, y_{tbn}, z_{tbn})$ can be expressed by the following equation:

$$P(x, y, z) = M_2 \times M_1 \times P^*(x_{tbn}, y_{tbn}, z_{tbn}) + \mathbf{S}(s_i) \tag{9}$$

In turn, we can obtain the correspondence between $P^*(x_{tbn}, y_{tbn}, z_{tbn})$ and $P(x, y, z)$, which is expressed by the following equation:

$$P^*(x_{tbn}, y_{tbn}, z_{tbn}) = (M_2 \times M_1)^{-1} \times (P(x, y, z) - \mathbf{S}(s_i)) \tag{10}$$

2. Establish the correspondence between $P^{\dagger}(x_{bnt}, y_{bnt}, z_{bnt})$ and $P^*(x_{tbn}, y_{tbn}, z_{tbn})$: according to the the definition of the extrusion path and the correspondence between the coordinate system **TBN** and **NBT**, the correspondence between $P^{\dagger}(x_{bnt}, y_{bnt}, z_{bnt})$ and $P^*(x_{tbn}, y_{tbn}, z_{tbn})$ can be expressed by the following equation:

$$\begin{cases} x_{bnt} = f_c(x_{tbn}, y_{tbn}) \\ y_{bnt} = z_{tbn} \\ z_{bnt} = x_{tbn} \end{cases} \tag{11}$$

3. Establish the correspondence between $P^{\dagger}(x_{bnt}, y_{bnt}, z_{bnt})$ and $P(x, y, z)$: according to the Equation 10 and 11, we can obtain the correspondence between $P^{\dagger}(x_{bnt}, y_{bnt}, z_{bnt})$ and $P(x, y, z)$, that is, the expression of distance mapping, which is denoted as the following equation:

$$\begin{cases} x_{bnt} = X(x, y, z) \\ y_{bnt} = Y(x, y, z) \\ z_{bnt} = Z(x, y, z) \end{cases} \tag{12}$$

References

[1] S. Appanaboyina, F. Mut, R. Lohner, C. Putman, and J. Cebral. Computational fluid dynamics of stented intracranial aneurysms using adaptive embedded unstructured grids. *International Journal for Numerical Methods in Fluids*, 57(5):475–493, 2008.

[2] M. Attene, M. Campen, and L. Kobbelt. Polygon mesh repairing: An application perspective. *Acm Computing Surveys*, 45(2):1–33, 2013.

[3] E. Bittar, N. Tsingos, and M. Gascuel. Automatic reconstruction of unstructured 3d data: Combining a medial axis and implicit surfaces. *Computer Graphics Forum*, 14(3):457–468, 1995.

[4] J. Bloomenthal. *Skeletal design of natural forms*. Phd thesis, 1995.

[5] J. Bloomenthal and K. Shoemake. Convolution surfaces. *Computer Graphics*, 25:251–256, 1991.

[6] A. Bornik, B. Reitinger, and R. Beichel. Reconstruction and representation of tubular structures using simplex meshes. In *Proc. of Winter School of Computer Graphics (WSCG)*, pages 61–65, 2005.

[7] J. Ding. *Numerical study on hemodynamics of cardiovascular surgical planning*. PhD thesis, 2013.

[8] C. Dong and G. Wang. Curvatures estimation on triangular mesh. *J Zhejiang Univ SCI*, 6A(Suppl. I):128–136, 2005.

[9] P. Dyverfeldt, M. Bissell, A. J. Barker, A. F. Bolger, C.-J. Carlhäll, T. Ebbers, C. J. Francios, A. Frydrychowicz, J. Geiger, D. Giese, et al. 4d flow cardiovascular magnetic resonance consensus statement. *Journal of Cardiovascular Magnetic Resonance*, 17(1):72, 2015.

[10] P. Felkel, l. Wegenkitt, and K. Buhler. Surface models of tube trees. In *Proc. of Computer Graphics International*, pages 70–77, 2004.

[11] H. Hahn, B. Preim, D. Selle, and H. Peitgen. Visualization and interaction techniques for the exploration of vascular structures. In *Proc. of IEEE Visualization*, pages 395–402, 2001.

[12] X. Han, R. Bibb, and R. Harris. Design of bifurcation junctions in artificial vascular vessels additively manufactured for skin tissue engineering. *Journal of Visual Languages and Computing*, 28(C):238–249, 2015.

[13] K. Höhne, B. Pflesser, and A. Pommert. A realistic model of the inner organs from the visible human data. In *Proc. of Medical Image Computing and Computer-Assisted Intervention*, pages 776–785, 2000.

[14] Q. Hong, L. Chen, B. Wang, and Q. Wu. The extraction of vascular axis based on signed distance function. In *International Conference on Graphic and Image Processing*, 2014.

[15] Q. Hong, Q. Li, and J. Tian. Implicit reconstruction of vasculatures using bivariate piecewise algebraic splines. *IEEE Transactions on Medical Imaging*, 31(3):543–553, 2012.

[16] Q. Hong, Q. Li, B. Wang, K. Liu, F. Lin, J. Lin, and et al. Accurate geometry modeling of vasculatures using implicit fitting with 2d radial basis functions. *Computer Aided Geometric Design*, 62:206 – 216, 2018.

[17] Q. Hong, Q. Li, B. Wang, K. Liu, and Q. Qi. High precision implicit modeling for patient-specific coronary arteries. *IEEE Access*, 7:72020–72029, 2019.

[18] R. Izzo, D. Steinman, S. Manini, and L. Antiga. The vascular modeling toolkit: a python library for the analysis of tubular structures in medical images. *Journal of Open Source Software*, 3(25):745, 2018.

[19] E. Kerrien, A. Yureidini, J. Dequidt, C. Duriez, R. Anxionnat, and S. Cotin. Blood vessel modeling for interactive simulation of interventional neuroradiology procedures. *Medical Image Analysis*, 35:685–698, 2017.

[20] A. Klepaczko, P. Szczypiński, A. Deistung, J. R. Reichenbach, and A. Materka. Simulation of mr angiography imaging for validation of cerebral arteries segmentation algorithms. *Computer methods and programs in biomedicine*, 137:293–309, 2016.

[21] A. Klepaczko, P. Szczypiński, M. Strzelecki, and L. Stefańczyk. Simulation of phase contrast angiography for renal arterial models. *Biomedical engineering online*, 17(1):41, 2018.

[22] J. Kretschmer, C. Godenschwager, B. Preim, and M. Stamminger. Interactive patient-specific vascular modeling with sweep surfaces. *IEEE Transactions on Visualization and Computer Graphics*, 19(12):2828–2837, 2013.

[23] Q. Li. Smooth piecewise polynomial blending operations for implicit shapes. *Computer Graphics forum*, 26(2):157–171, 2007.

[24] Q. Li, Q. Hong, Q. Qi, X. Ma, X. Han, and J. Tian. Towards additive manufacturing oriented geometric modeling using implicit functions. *Visual Computing for Industry, Biomedicine, and Art*, 1(1):1–9, 2018.

[25] Q. Li and J. Tian. 2d piecewise algebraic splines for implicit modeling. *ACM Transactions on Graphics*, 28(2):13, 2009.

[26] Q. Li and J. Tian. Partial shape-preserving splines. *Computer-Aided Design*, 43(4):394–409, 2011.

[27] Q. Li, D. Wills, R. Phillips, W. J. Viant, J. G. Griffiths, and J. Ward. Implicit fitting using radial basis functions with ellipsoid constraint. *Computer Graphics Forum*, 23(1):55–69, 2004.

[28] Y.-j. Liu, R.-q. Qiu, and X.-h. LIANG. Nurbs curve blending using extension. *Journal of Zhejiang University Science A*, 10(4):570–576, 2009.

[29] A. L. Marsden. Optimization in cardiovascular modeling. *Annual Review of Fluid Mechanics*, 46(1):519–546, 2014.

[30] I. Marshall. Computational simulations and experimental studies of 3d phase-contrast imaging of fluid flow in carotid bifurcation geometries. *Journal of Magnetic Resonance Imaging: An Official Journal of the International Society for Magnetic Resonance in Medicine*, 31(4):928–934, 2010.

[31] Y. Masutani, K. Masamune, and T. Dohi. Region-growing-based feature extraction algorithm for tree-like objects. In *Proc. of Visualization in Biomedical Computing*, pages 161–171, 1996.

[32] S. Oeltze and B. Preim. Visualization of vascular structures with convolution surfaces: Method, validation and evaluation. *IEEE Transactions on Medical Imaging*, 25(3):540–549, 2005.

[33] Y. Ohtake, A. Belyaev, M. Alexa, G. Turk, and H. Seidel. Multilevel partition of unity implicits. *ACM Transactions on Graphics*, 22:463–470, 2003.

[34] S. Petersson, P. Dyverfeldt, R. Gårdhagen, M. Karlsson, and T. Ebbers. Simulation of phase contrast mri of turbulent flow. *Magnetic resonance in medicine*, 64(4):1039–1046, 2010.
[35] B. Preim and S. Oeltze. 3d visualization of vasculature: An overview. *Visualization in Medicine and Life Science*, pages 39–59, 2007.
[36] A. N. Pressley. *Elementary differential geometry*. Springer Science & Business Media, 2010.
[37] P. Saalfeld, A. Baer, U. Preim, B. Preim, and K. Lawonn. Sketching 2d vessels and vascular diseases with integrated blood flow. In *Proceedings of 10th International Conference on Computer Graphics Theory and Applications*, 03 2015.
[38] C. Schumann, M. Neugebauer, R. Bade, H.-O. Peitgen, and B. Preim. Implicit vessel surface reconstruction for visualization and cfd simulation. *International Journal of Computer Assisted Radiology and Surgery*, 2(5):275–286, 2008.
[39] C. Schumann, S. Oeltze, R. Bade, B. Preim, and H.-O. Peitgen. Model-free surface visualization of vascular trees. In *Proc. of IEEE/Eurographics Symposium on Visualization*, pages 283–290, 2007.
[40] N. Tsingos, E. Bittar, and M.-P. Gascuel. Implicit surfaces for semi-automatic medical organ reconstruction. *Computer Graphics International95*, pages 3–15, 1995.
[41] B. Urick, T. M. Sanders, S. S. Hossain, Y. J. Zhang, and T. J. Hughes. Review of patient-specific vascular modeling: template-based isogeometric framework and the case for cad. *Archives of Computational Methods in Engineering*, 26(2):381–404, 2019.
[42] X. Wang, Z. Wu, J. Shen, T. Zhang, X. Mou, and M. Zhou. Repairing the cerebral vascular through blending ball b-spline curves with g 2 continuity. *Neurocomputing*, 173:768–777, 2016.
[43] WHO. World health statistics, 2017. [Online] Available: https://www.west-info.eu/fake-news-on-vaccines-means-italy-lags-behind-poorer-countries/who-world-health-statistics-2017/. Accessed April 4, 2019.
[44] J. Wu, R. Ma, X. Ma, F. Jia, and Q. Hu. Curvature-dependent surface visualization of vascular structures. *Computerized Medical Imaging and Graphics*, 34(8):651–658, 2010.
[45] J. Wu, M. Wei, Y. Li, X. Ma, F. Jia, and Q. Hu. Scale-adaptive surface modeling of vascular structures. *Biomedical engineering online*, 9(1):75, 2010.
[46] X. Wu, V. Luboz, K. Krissian, S. Cotin, and S. Dawson. Segmentation and reconstruction of vascular structures for 3d real-time simulation. *Medical Image Analysis*, 15(1):22–34, 2011.
[47] G. Xiong, G. Choi, and C. A. Taylor. Virtual interventions for image-based blood flow computation. *Computer-Aided Design*, 44:3–14, 2012.
[48] Y. Zhang, Y. Bazilevs, S. Goswami, C. L. Bajaj, and T. J. R. Hughes. Patient-specific vascular nurbs modeling for isogeometric analysis of blood flow. *Computer Methods in Applied Mechanics and Engineering*, 196(29-30):2943–2959, 2007.
[49] Y. Zhang, B. Matuszewski, L. Shark, and C. Moore. Medical image segmentation using new hybrid level-set method. In *Proceedings of Fifth International Conference BioMedical Visualization: Information Visualization in Medical and Biomedical Informatics*, pages 71–76, 2008.